Electrically tunable resonant scattering in fluorinated bilayer graphene

Adam A. Stabile, Aires Ferreira, Jing Li, N. M. R. Peres, and J. Zhu

Phys. Rev. B **92**, 121411 — Published 28 September 2015

DOI: 10.1103/PhysRevB.92.121411

Electrically tunable resonant scattering in fluorinated bilayer graphene

Adam A. Stabile[1], Aires Ferreira[2,3],* Jing Li[1], N. M. R. Peres[3], and J. Zhu[1]†
[1] *Department of Physics, The Pennsylvania State University, University Park, Pennsylvania 16802, USA*
[2] *Department of Physics, University of York, York YO10 5DD, United Kingdom and*
[3] *Centro de Fisica and Departamento de Fisica, Universidade do Minho, Campus de Gualtar, Braga 4710-057, Portugal*

Adatom-decorated graphene offers a promising new path towards spintronics in the ultra-thin limit. We combine experiment and theory to investigate the electronic properties of dilutely fluorinated bilayer graphene, where the fluorine adatoms covalently bond to the top graphene layer. We show that fluorine adatoms give rise to resonant impurity states near the charge neutrality point of the bilayer, leading to strong scattering of charge carriers and hopping conduction inside a field-induced band gap. Remarkably, the application of an electric field across the layers is shown to tune the resonant scattering amplitude from fluorine adatoms by nearly two-fold. The experimental observations are well explained by a theoretical analysis combining Boltzmann transport equations and fully quantum-mechanical methods. This paradigm can be generalized to many bilayer graphene–adatom materials and we envision that the realization of electrically tunable resonance may be a key advantage in graphene-based spintronic devices.

PACS numbers: 72.80.Vp, 72.10.Fk

Chemical functionalization is a powerful tool to engineer graphene for a broad range of application needs. Attachment of oxygen groups makes graphene soluble and fluorescent, and facilitates the formation of graphene nanocomposites [1–3]. Chemisorbed species increase the degree of sp^3 bonding, drastically affecting graphene's electrical conductivity, mechanical strength, and optical response, even in the very dilute limit [4–22]. Deposition of light adatoms, such as hydrogen and fluorine, endows graphene with intriguing magnetic and spintronic properties, including localized magnetic moments and enhanced spin-orbit coupling, which may enable the generation of large spin current [16–19, 21–24].

Covalently bonded monovalent species, with orbitals close to the Dirac point of graphene systems, effectively decouple their carbon host from its neighbors, thereby simulating vacancies [25]. The latter are predicted to introduce power-law localized midgap states at the Dirac point [26–28], displaying anomalous divergent behavior of the density of states [29, 30]. These so-called resonant scatterers have a profound impact on charge carrier transport at all carrier densities, invalidating conventional transport pictures based on the weak disorder hypothesis [31–33]. In the high carrier density regime $|n| \gg n_{\rm rs}$, where $n_{\rm rs}$ denotes the areal density of resonant scatterers, the dc-conductivity deviates from its typical behaviour $\sigma \propto |n|$, acquiring a robust sublinear dependence, owing to a non-perturbative renormalization of s-wave phase-shifts: $\delta_0(n) \approx \pi/[2\ln(R\sqrt{\pi|n|})]$, where $R \approx 0.4$ nm is the scatterer range [18, 25, 31, 32].

Resonant scattering also plays an important role in metal spintronics [34], although such interactions are not easily tunable. Engineering tunable resonant interaction of charge carriers with atomic impurities in graphene *in situ* would open new avenues, including the harnessing of spin relaxation [35] and generation of robust spin currents through extrinsic spin Hall effect [23, 24]. From the viewpoint of device scaling and operations, it is particular desirable to implement gate-controlled resonant interactions. A suitable candidate—so far overlooked—is bilayer graphene (BLG). Adatoms in BLG are likewise predicted to induce resonant scattering [32, 36, 37]. Moreover, the presence of two layers allows the mirror symmetry to be broken by an electric field perpendicular to the layers, opening up a band gap up to 250 meV [38–42]. The consequences of this extra degree of freedom for resonant scattering remain largely unexplored.

In this Letter, we report the first experimental observations of adatom-limited charge transport in BLG using fluorine adatoms as an example. Dual-gating allows us to control the carrier type, density and the perpendicular (bias) electric field independently. Both experiment and theory demonstrate that fluorine adatoms behave as resonant scatterers. Moreover, we show that the charge carrier scattering amplitude becomes strongly electron-hole asymmetric and is tunable over a large range $\pm 20-30\%$ by controlling the carrier distribution between the two layers using a bias electric field. Once more, theory and experiment are found to be in excellent agreement. The demonstrated electric tunability of the resonant cross section offers a convenient tool to engineer desired charge–spin responses in graphene–adatom systems.

Bilayer graphene flakes are exfoliated from bulk HOPG graphite (ZYA grade, SPI supplies) onto prefabricated HfO2/Au bottom gate stacks [43], optically identified and confirmed by Raman spectroscopy. The flakes are then fluorinated in a CF_4 plasma asher where fluorine atoms covalently bond with carbon atoms in the top layer only [see Fig. 1(a)]. Bilayer graphene is substantially harder to fluorinate compared to monolayer graphene [17]. Discussions of the plasma conditions are given in the Supplementary Material (SM). After fluorination, ver der

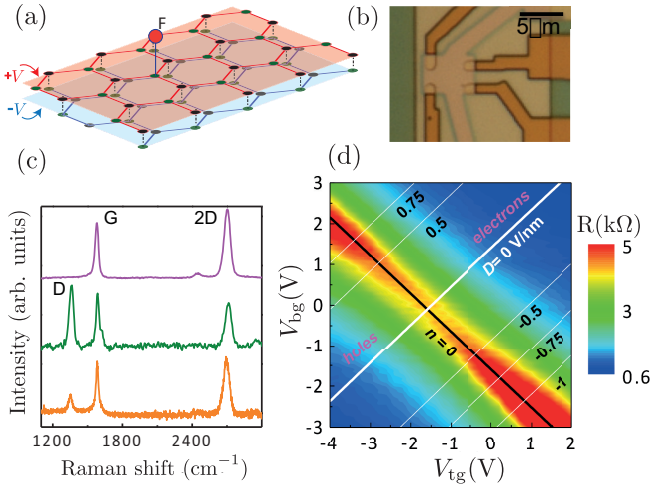

Figure 1: Single-sided fluorinated BLG. (a) Schematic. Full (dashed) lines represent the intra-layer (inter-layer) hopping terms. Fluorine adatoms bond to carbon hosts at random positions. (b) Optical micrograph of sample W02 showing the Au bottom gate (wide yellow stripe), four Au electrodes to the sample (dark gold) in van der Pauw geometry and the top gate connected to two Au electrodes (yellow). (c) Raman spectra of pristine (plum), fluorinated (olive, from sample W02) and defluorinated (orange) BLG. The laser excitation wavelength is 488 nm. I_D/I_G=1.15 for W02 and 0.3 for the defuorinated sample. (d) The color map of a four-terminal resistance R as a function of the top and bottom gate voltages. The black line corresponds to n=0 and the white lines correspond to constant bias D fields. T=10 K. From W38.

Pauw or Hall bar devices are completed using standard e-beam lithography and atomic layer deposition techniques [42, 43]. Results from three fluorinated samples (W02, W03, and W38) and one defluorinated sample Df are reported here. An optical micrograph of device W38 is shown in Fig. 1(b). Fig. 1(c) plots the Raman spectra of a pristine bilayer, device W02, and a typical trace from a defluorinated bilayer; see SM and Ref. [17] for defluorination recipe. Following the atomic defect density calibration obtained by Lucchese *et al.* on monolayers [44] and taking into account the doubling of the G band intensity in bilayer, we estimate a fluorine areal density $n_{\rm F}^{\rm ram} \approx 3.3\times10^{12}$ cm^{-2} for device W02, and the unintentional defect density (e.g. vacancy), as seen in the defluorinated bilayer, is roughly 0.6×10^{12} cm^{-2}. Parameters from all four samples are given in Table I of the SM. We use standard low-frequency, low excitation lock-in techniques to carry out electrical transport measurements at temperatures ranging from 1.6 K to 200 K. A false color map of a four-terminal resistance R in sample W38 as a function of the top and bottom gate voltages $V_{\rm tg}$ and $V_{\rm bg}$ is shown in Fig. 1 (d) and displays characteristics similar to that of pristine bilayer [42]. This map enables us to extract the dependence of the sheet conductance σ_s on the carrier density n at fixed bias D-fields.

Resonant impurity scattering.—We first establish the resonant impurity nature of the fluorine adatoms. The rearrangement of electronic spectral weight due to the fluorination can be estimated through a calculation of the density of states (DOS) for a typical adatom concentration. To model the BLG system we employ a nearest-neighbor tight-binding Hamiltonian of π-electrons, supplemented with a on-site energy term $\pm V$ in the top (bottom) layer describing the effect of the D-field. Fluorine adatoms are modeled as vacancies in the top layer [25, 32]. The kernel polynomial method [45] is then used to accurately extract the DOS of a large lattice with 2×14142^2 carbon atoms. Details of the calculation are given in the SM. The DOS is shown in Fig. 2(a). We note two prominent features of the DOS.

In unbiased BLG, the DOS displays a sharp peak centered at zero energy (midgap state), already encountered in Refs. [32, 46]. At non-zero bias field, new resonances pile up at the edges of the pseudo-gap, which is consistent with results obtained for a single vacancy [28]. Due to the broken layer symmetry, these resonances have different weights at $E_F \approx \pm V$, anticipating substantial electron-hole asymmetry (EHA). Fig. 2(b) shows $\sigma_{\rm s}(n)$ at $D = 0$ for samples W38, W02, W03 and Df at T =1.6 K. Sample Df has a field effect mobility of $\mu \approx$1600 cm^2/Vs, which is comparable to that of pristine bilayer in a similar geometry [42]. In contrast, fluorinated bilayers display much lower mobility: 172, 100, 86 cm^2/Vs for W38, W02 and W03 respectively, which signals the dominance of adatom-induced scattering. Ferreira et al. [32] showed that in the high carrier density regime $n > n_{\rm F}$ where quantum corrections are not dominant, semiclassical description applies and the resonant-scattering-limited sheet conductivity in unbiased BLG is given by

$$\sigma_{\rm s}(n) = 2\times\frac{\pi e^2}{4h}\frac{|n|}{n_{\rm F}}, \qquad (1)$$

where an extra factor of 2 accounts for the one-sided fluorination of our samples. Since $\sigma_{\rm s}$ is approximately insensitive to the scatterer radius, there is a single fitting parameter, $n_{\rm F}$. Fits to Eq. 1 are plotted as dashed lines in Fig. 2(b) and describe data very well at high density [32]. The extracted $n_{\rm F}$ are in good agreement with values obtained from Raman spectra for all samples (see Table I in SM). Furthermore, in all samples we find an n_F-independent $\sigma_{\rm s} \approx e^2/h$ in the low carrier density regime $n < n_{\rm F}$, also in agreement with theory. This observation is consistent with the formation of a narrow "impurity band" around the CNP [32, 46] [see thick (orange) line in Fig. 2(a)].

More direct evidence of the impurity band is seen in the temperature-dependent resistance of the CNP under a finite bias field. Figure 3(a) plots $R_{\rm CNP}(D)$—the sheet resistance of the CNP in sample W02—as a function of D

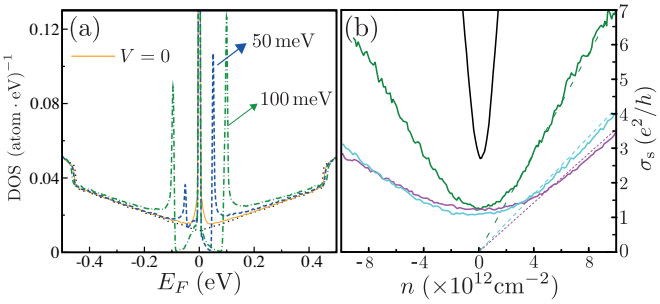

Figure 2: Resonant impurity scattering in fluorinated BLG. (a) Calculated DOS of macroscopic size ($\approx \mu$m^2) BLG system as a function of the Fermi energy at selected bias potential values for F : C ratio 1 : 2000. The DOS of pristine unbiased BLG is also shown (dotted line). (b) $\sigma_s(n)$ in samples (from top to bottom): Df (black), W38 (olive), W02 (cyan) and W03 (plum) at $T = 1.6$ K. Positive n corresponds to electron doping. Dashed lines of the same color are fits to Eq. (1).

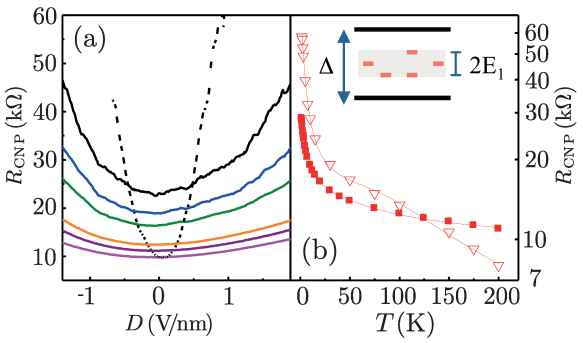

Figure 3: Charge carrier transport at the CNP. (a) R_s vs. D at the CNP for sample Df (dashed line, T=1.6 K) and sample W02 (solid lines). From top to bottom: T=1.6 K(black), 5 K (blue), 10 K (olive), 50 K(orange), 100 K(purple) and 200 K (plum). (b) $R_S(T)$ of sample Df (hollow triangles) and sample W02 (solid squares) at D=0.93 V/nm. The solid lines are fits to Eq.(1) of Ref. [42]. E_1= 11 meV and 33.5 meV for samples W02 and Df, respectively. Inset: a schematic diagram of the fluorine induced impurity states inside the field-induced band gap of a bilayer graphene.

at selected temperatures T =1.6 to 200 K, together with $R_{\rm CNP}(D)$ of sample Df at T =1.6 K. $R_{\rm CNP}(D)$ of sample Df is similar to that of pristine bilayer [42]. $R_{\rm CNP}(D)$ of W02, on the other hand, rises much more slowly, pointing to additional conduction channels inside the band gap. To further understand the behavior of $R_{\rm CNP}$, we plot in Fig. 3(b) its temperature dependence in both samples at D =0.93 V/nm. The most remarkable difference between the two lies at high temperatures $T > 50$ K. In this regime, sample Df exhibits activated transport $R_1 \propto \exp(E_1/k_BT)$, with E_1 increasing with D from 22.5 meV at $D = 0$ (data not shown) to 33.5 meV at $D = 0.93$ V/nm. These values are similar to pristine bilayers, where $\Delta = 2E_1$ approximates the bias-induced band gap in the large D limit [42]. In contrast, similar analyses done on $R_{\rm CNP}(T)$ of the three fluorinated bilayers yield roughly D-independent E_1, which is approximately 11-13 meV in all samples. We attribute this behavior to nearest neighbor hopping among the fluorine-induced impurity states as illustrated in the inset to Fig. 3(b), where E_1 is the half width of the impurity band. This mechanism effectively shunts the band edge activation $\exp(\Delta/2k_BT)$ to result in an D-independent $R_{\rm CNP}(T)$. Counting two impurity states per adatom [32], we independently estimate the bandwidth to be ≈10 meV at $n_{\rm F} \approx 4 \times 10^{12}$ cm^{-2}, which is in excellent agreement with the E_1 values extracted here.

Electric-field tuning of resonant scattering.—Next, we explore the role of a bias D field in the carrier density regime $n > n_{\rm F}$. Figure 4(a) plots $\sigma_s(n)$ of sample W02 at selected D's from -2 to 2 V/nm, where $D > 0$ indicates field pointing towards the fluorine adatoms as the inset of (a) shows. Pronounced EHA is observed. For electrons, σ_s increases (decreases) when $D > 0$ $(D < 0)$ and the opposite trend is observed for holes. This D-field tuning is further illustrated in Fig. 4(b), where we plot the normalized conductance change $\delta\sigma_s(D) \equiv \Delta\sigma_s(D)/\sigma_s(0) = [\sigma_s(D)-\sigma_s(0)]/\sigma_s(0)$ of data in Figure 4 (a). Strikingly, in the high-density regime, $\delta\sigma_s(D)$ is roughly n-independent and ranges between -0.35 and 0.2 for $|D| < 2$ V/nm, i.e., the change of σ_s is nearly two-fold. Furthermore, $\delta\sigma_s(D)$ appears to be symmetric under $(n, D) \to (-n, -D)$. Similar D-field tuning of $\sigma_s(n)$ is observed on all three fluorinated samples, with the magnitude of $\delta\sigma_s(D)$ varying within a factor of 2 among them. Further examination of the EHA rules out an extrinsic mechanism due to non-uniform density distribution created by electrodes that screen a portion of the top gate. The detailed discussions are given in the SM. Intuitively, the experimental observations suggest increased distribution of hole (electron) wave function in the top layer under a positive (negative) D field, and thus increased resonant impurity scattering.

To gain further insight into the strong D field tuning of charge carrier transport, we solve analytically the Boltzmann transport equations for a BLG system with random short-range impurities constrained to one layer. We posit our investigations in the four-band continuum BLG–adatom Hamiltonian

$$\hat{H} = \begin{pmatrix} V + v_F\boldsymbol{\sigma}\cdot\hat{\mathbf{p}} & t_\perp\sigma_- \\ t_\perp\sigma_+ & -V + v_F\boldsymbol{\sigma}\cdot\hat{\mathbf{p}} \end{pmatrix} + \sum_i \begin{pmatrix} v_0^i(\mathbf{r}) & 0 \\ 0 & 0 \end{pmatrix}, \quad (2)$$

where $\hat{\mathbf{p}}$ is the 2D kinematic momentum operator around Dirac point K, $v_F \approx 10^6$ m/s is the Fermi velocity, $\boldsymbol{\sigma}$ are Pauli matrices, with $\sigma_z = \pm 1$ describing states residing on the $A(B)$ sublattice, and $\sigma_\pm = \sigma_x \pm i\sigma_y$. The diagonal blocks in the first term on the RHS describe monolayers at constant electrostatic energy, $\pm V$ for top layer and bottom layer, respectively, whereas off-diagonal blocks contain the hopping processes $A_2 \rightleftharpoons B_1$ connecting the two layers ($t_\perp \approx 0.45$ eV) [47]. The bias potential V is

determined from the experimental parameters according to $V = -eDd/2\kappa$, where $-e < 0$ is the electron's charge, $d \approx 0.35$ nm is the layer separation, and $\kappa = 4$ is the phenomenological BLG effective permittivity [39, 48]. Diagonalization of the first term yields 2+2 bands separated by a gap: $\Delta = 2|V|t_\perp/\sqrt{t_\perp^2 + 4V^2} \approx 2|V|$. Their dispersion relation reads $\epsilon^{\pm\pm}(\boldsymbol{\pi}) = \pm\sqrt{t_\perp^2/2 + \boldsymbol{\pi}^2 + V^2 \pm \lambda^2(\boldsymbol{\pi})}$, where $\boldsymbol{\pi} \equiv v_F\mathbf{p}$ and $\lambda^2(\boldsymbol{\pi}) = \sqrt{t_\perp^4/4 + \boldsymbol{\pi}^2\,(t_\perp^2 + 4V^2)}$. The second term is the scattering potential due to fluorine adatoms located in the top layer at random positions $\{\mathbf{r}_i\}$ with $v_0^i(\mathbf{r}) = v_0\delta(\mathbf{r} - \mathbf{r}_i)$. In the scattering problem, outgoing and incoming wavefunctions are related by the T matrix [49]. For delta-peak potentials, outgoing waves from a single impurity at the origin acquires the simple form $\psi_{\rm scatt}(\mathbf{r}) = \hat{G}_0(\mathbf{r}, E)\hat{T}_{\rm ad}(E)\phi_{\mathbf{k}}(\mathbf{r})$, where $\phi_{\mathbf{k}}(\mathbf{r})$ denotes free incoming wave solutions with momentum $\mathbf{k}$, i.e., $\hat{H}_0|\phi_{\mathbf{k}}\rangle = E|\phi_{\mathbf{k}}\rangle$, and $\hat{G}_0(\mathbf{r}, E)$ is the propagator of pristine biased BLG, $\hat{G}_0(\mathbf{r}, E) = \langle\mathbf{r}|(E - \hat{H}_0 + i\eta)|\vec{0}\rangle$, with η a real infinitesimal. In the (resonant) scattering limit of interest $v_0 \to \infty$, we easily find

$$\hat{T}_{\rm ad}(E) = -\sum_{\chi=A_2,B_2} [g_\chi(E)]^{-1}|\chi\rangle\langle\chi|\,, \qquad (3)$$

where $g_\chi(E) \equiv \langle\chi|\hat{G}(\vec{0}, E)|\chi\rangle$. We evaluated $g_\chi(E)$ in the entire parameter space (refer to SM); in the intermediate regime $\sqrt{t_\perp^2 + V^2} > |E| > |V|$ (typically ∼0.05–0.5 eV),

$$g_{A_2}(E) = (V - E)\left[\bar{\Theta}_\Lambda(E) + (E + V)^2\Theta_{\rm reg}(E)\right]\,, \qquad (4)$$

$$g_{B_2}(E) = (t_\perp^2 + V^2 - E^2)(E + V)\Theta_{\rm reg}(E) + (V - E)\bar{\Theta}_\Lambda(E)\,, \qquad (5)$$

where

$$\left\{\begin{array}{c}\Theta_{\rm reg}(E)\\ \bar{\Theta}_\Lambda(E)\end{array}\right\} = \frac{1}{4\pi v_F^2}\frac{1}{A_+ + A_-}\left\{\begin{array}{c}\ln\left(\frac{A_+}{A_-}\right) - i\pi\\ \Psi(\Lambda) + i\pi A_+\end{array}\right\}. \qquad (6)$$

In the above, $A_\pm = \sqrt{4E^2V^2 + t_\perp^2(E^2 - V^2)} \pm (E^2 + V^2)$, $\Psi(x) = \sum_{p=\pm1} A_p \ln(-p + x^2/|A_p|)$, and $\Lambda = \hbar v_F/R$ is the high-energy cutoff defining an effective potential range R [32]. Crucially, for non-zero bias field $|V| > 0$, the T matrix is sensitive to carrier polarity $\pm|E|$ [see Eqs. (4)–(5)]. This feature results from the top-bottom layer asymmetry induced by the adatoms and, as argued below, is the origin of the strong EHA observed.

The effect of dilute random adatoms in dc-transport is encoded in the inverse transport relaxation time

$$\frac{1}{\tau(\mathbf{k})} = \frac{2\pi n_{\rm F}}{\hbar}\int\frac{d^2\mathbf{k}'}{(2\pi)^2}|\langle\phi_{\mathbf{k}}|\hat{T}_{\rm ad}(E)|\phi_{\mathbf{k}'}\rangle|^2\delta_{\mathbf{k}\mathbf{k}'}(E)\,, \qquad (7)$$

where $\delta_{\mathbf{k}\mathbf{k}'}(E) \equiv (1 - \cos\theta_{\mathbf{k}\mathbf{k}'})\delta(\epsilon_{\mathbf{k}} - \epsilon_{\mathbf{k}'})$, $\theta_{\mathbf{k}\mathbf{k}'}$ is the scattering angle, and $\epsilon_{\mathbf{k}} \equiv \epsilon^{\pm-}(v_F\hbar\mathbf{k})$ for $E = \pm|E|$. The zero-temperature semiclassical dc-conductivity follows from $\sigma_{\rm s} = (e^2/h)k_F v(k_F)\tau(k_F)$, where $v(k) = |\nabla_k\epsilon_k|/\hbar$ is the band velocity and k_F is the Fermi wavevector [50]. In order to unbiasedly extract the model parameters $n_{\rm F}$ and R, we fit the 4-band expression to the $D = 0$ conductivity data in the electron sector $n > 0$ [see black curve in Fig. 4 (a)]. We obtain $n_{\rm F} \approx 1.6n_{\rm F}^{\rm ram}$ and $R \approx 0.5$ nm, where $n_{\rm F}^{\rm ram}$ is obtained from the Raman spectra of this device (see above). These parameters are then employed to evaluate $\sigma_{\rm s}(n)$ at all non-zero D-fields in Fig. 4 (c). The theory is seen to reproduce very well both the degree of EHA and the overall D-dependence observed in panel (a). This agreement is particularly remarkable as the strong scattering regime is characterized by a strong dependence of $\tau^{-1}(\mathbf{k})$ in the D-field and model parameters. This robust agreement is strong evidence that the D-field tuning of the resonant adatom scattering amplitudes (3) is responsible for the observed conductance modulation. Because of the resonant nature of the adatoms, a two-fold change of the scattering cross section can lead to very large tuning of other resonant properties such as the spin Hall angle [23], giving BLG-based systems a distinct advantage in graphene-based spintronics.

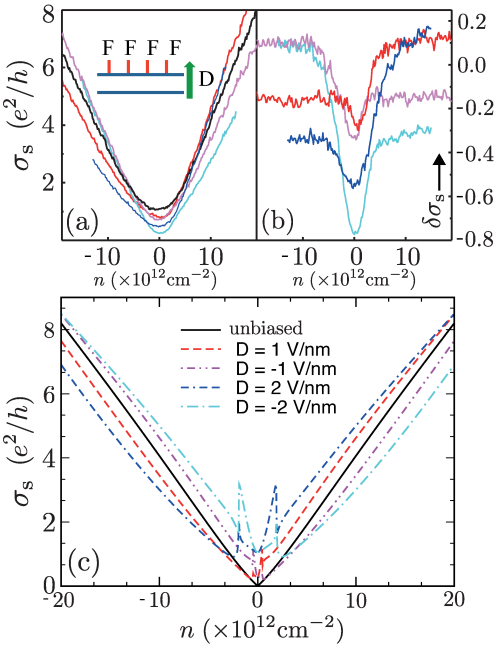

Figure 4: Tuning of charge carrier transport in D-field. (a) and (b) $\sigma_{\rm s}(n)$ and normalized conductance change $\delta\sigma_s(D)$ for W02 at $T = 1.6$ K and D =-2 V/nm (cyan), -1 V/nm (plum), 0 V/nm (black), 1 V/nm (red), and 2 V/nm (blue). Positive D points towards the fluorine adatoms as illustrated in the inset of(a). (c) Calculated dc-conductivity $\sigma_{\rm s}(n)$ for several inter-layer bias potentials corresponding to the $D-$field values in (a). Calculation only applies to $n > n_F$. Other parameters in main text.

In summary, through a joint experiment–theory effort, we have demonstrated that a perpendicular electric field achieves substantial tuning of the amplitude of

resonant impurity scattering in one-sided fluorinated bilayer graphene. Our findings set the stage for exploring all-electric control of resonant scatterings that underlie novel spintronics effects in graphenic materials.

Acknowledgements. We thank X. Hong for helpful discussions. A.S., J.L. and J.Z. are supported by ONR under grant no. N00014-11-1-0730 and by NSF CAREER grant no. DMR-0748604. A.F. and N.M.R.P. acknowledge EC under Graphene Flagship (Contract No. CNECT-ICT-604391). A.F. is supported by the Royal Society University Research Fellowship scheme. We acknowledge use of facilities at the PSU site of NSF NNIN.

* Electronic address: aires.ferreira@york.ac.uk
† Electronic address: jzhu@phys.psu.edu

[1] S. Stankovich, D. A. Dikin, G. H. B. Dommett, K. M. Kohlhaas, E. J. Zimney, E. A. Stach, R. D. Piner, S. T. Nguyen, and R. S. Ruoff, Nature **442**, 282 (2006).
[2] Z. Luo, P. Vora, E. Mele, A. Johnson, and J. Kikkawa, Appl. Phys. Lett. **94**, 111909 (2009).
[3] G. Eda, and M. Chhowalla, Advanced Materials **22**, 2392 (2010).
[4] D. Elias, R. Nair, T. Mohiuddin, S. Morozov, P. Blake, M. Halsall, A. Ferrari, D. Boukhvalov, M. Katsnelson, and A. Geim, Science **323**, 610 (2009).
[5] S. H. Cheng, K. Zou, F. Okino, H. Gutierrez, A. Gupta, N. Shen, P. Eklund, J. Sofo, and J. Zhu, Phys. Rev. B **81**, 205435 (2010).
[6] B. Wang, J. R. Sparks, H. R. Gutierrez, F. Okino, Y Tang, V. H. Crespi, J. O. Sofo and J. Zhu, Appl. Phys. Lett. **97**, 141915 (2010).
[7] J. T. Robinson, J. S. Burgess, C. E. Junkermeier, S. C. Badescu, T. L. Reinecke, F. K. Perkins, M. K. Zalalutdniov, J. W. Baldwin, J. C. Culbertson, P. E. Sheehan, and E. S. Snow, Nano Lett. **10**, 3001 (2010).
[8] R. R. Nair, W. C. Ren, R. Jalil, I. Riaz, V. G. Kravets, L. Britnell, P. Blake, F. Schedin, A. S. Mayorov, S. J. Yuan, M. I. Katsnelson, H. M. Cheng, W. Strupinski, L. G. Bulusheva, A. V. Okotrub, I. V. Grigorieva, A. N. Grigorenko, K. S. Novoselov, and A. K. Geim, Small **6**, 2877 (2010).
[9] Z. H. Ni, L. A. Ponomarenko, R. R. Nair, R. Yang, S. Anissimova, I. V. Grigorieva, F. Schedin, P. Blake, Z. X. Shen, E. H. Hill, K. S. Novoselov, and A. K. Geim, Nano Lett. **10**, 3868 (2010).
[10] O. Leenaerts, H. Peelaers, A. Hernandez-Nieves, B. Partoens, and F. Peeters, Phys. Rev. B **82**, 195436 (2010).
[11] J.-H. Chen, W. G. Cullen, C. Jang, M. S. Fuhrer, and E. D. Williams, Phys. Rev. Lett. **102**, 236805 (2009)
[12] M. Klintenberg, S. Lebegue, M. I. Katsnelson, and O. Eriksson, Phys. Rev. B **81**, 085433 (2010).
[13] H. Zhang, E. Bekyarova, J. W. Huang, Z. Zhao, W. Bao, F. Wang, R. C. Haddon, and C. N. Lau, Nano Lett. **1**, 4047 (2011).
[14] F. Withers, T. H. Bointon, M. Dubois, S. Russo, and M. Craciun, Nano Lett. **11**, 3912 (2011).
[15] B. Wang, J. Wang, and J. Zhu, ACS Nano **8**, 1862 (2014).
[16] O. Yazyev, Rep. Prog. Phys. **73**, 056501 (2010).
[17] X. Hong, S. H. Cheng, C. Herding, and J. Zhu, Phys. Rev. B **83**, 085410 (2011).
[18] X. Hong, K. Zou, B. Wang, S. H. Cheng, and J. Zhu, Phys. Rev. Lett. **108**, 226602 (2012).
[19] R. Nair, M. Sepioni, I.-L. Tsai, O. Lehtinen, J. Keinonen, A. Krasheninnikov, T. Thomson, and A. Grigorieva, Nat. Phys. **8**, 199 (2012).
[20] J.-H. Chen, L. Li, W. G. Cullen, E. D. Williams, M. S. Fuhrer, Nat. Phys. **7**, 535 (2011).
[21] K. M. McCreary, A. G. Swartz, W. Han, J. Fabian, and R. K. Kawakami, Phys. Rev. Lett. **109**, 186604 (2012).
[22] J. Balakrishnan, G. Kok Wai Koon, M. Jaiswal, A. H. Castro Neto, and B. Ozyilmaz, Nat. Phys. **9**, 284 (2013).
[23] A. Ferreira, T.G. Rappoport, M.A. Cazalilla, and A.H. Castro Neto, Phys. Rev. Lett. **112**, 066601 (2014).
[24] J. Balakrishnan, G.K.W. Koon, A. Avsar, Y. Ho, J.H. Lee, M. Jaiswal, S.-J. Baeck, J.-H. Ahn, A. Ferreira, M.A. Cazalilla, A.H. Castro Neto, B. Ozyilmaz, Nat. Comm. **5**, 4748 (2014).
[25] T. O. Wehling, M. I. Katsnelson, and A. I. Lichtenstein, Chem. Phys. Lett. **476**, 125 (2009).
[26] V. M. Pereira, F. Guinea, J. M. B. Lopes dos Santos, N. M. R. Peres, and A. H. Castro Neto. Phys. Rev. Lett. **96**, 036801 (2006).
[27] V. M. Pereira, J. M. B. Lopes dos Santos, and A. H. Castro Neto. Phys. Rev. B **77**, 115109 (2008).
[28] E. V. Castro, M. P. L.-Sancho, and M. A. H. Vozmediano, Phys. Rev. Lett. **104**, 036802 (2010).
[29] V. Haefner, J. Schindler, N. Weik, T. Mayer, S. Balakrishnan, R. Narayanan, S. Bera, and F. Evers, Phys. Rev. Lett. **113**, 186802 (2014).
[30] P. M. Ostrovsky, I. V. Protopopov, E. J. Konig, I. V. Gornyi, A. D. Mirlin, and M. A. Skvortsov, Phys. Rev. Lett. **113**, 186803 (2014).
[31] T. Stauber, N. M. R. Peres, and F. Guinea, Phys. Rev. B **76**, 205423 (2007).
[32] A. Ferreira, J. Viana-Gomes, J. Nilsson, E. R. Mucciolo, N. M. R. Peres, and A. H. Castro Neto, Phys. Rev. B **83**, 165402 (2011).
[33] A. Ferreira, and E. R. Mucciolo, arXiv:1507.00488; to appear in PRL (2015).
[34] A. Fert, and P. M. Levy, Phys. Rev. Lett. **106**, 157208 (2011); Y. Niimi, M. Morota, D.H. Wei, C. Deranlot, M. Basletic, A. Hamzic, A. Fert, and Y. Otani. *ibidem* 126601 (2011).
[35] D. Kochan, M. Gmitra, and J. Fabian, Phys. Rev. Lett. **112**, 116602 (2014).
[36] R. E. Mapasha, A. M. Ukpong, and N. Chetty, Phys. Rev. B **85**, 205402 (2012).
[37] D. Nafday, and T. Saha-Dasgupta, Phys. Rev. B **88**, 205422 (2013).
[38] E. McCann, Phys. Rev. B **74**, 161403 (2006).
[39] H. K. Min, B. Sahu, S. K. Banerjee, and A. H. MacDonald, Phys. Rev. B **75**, 155115 (2007).
[40] Y. B. Zhang, T. T. Tang, C. Girit, Z. Hao, M. C. Martin, A. Zettl, M. F. Crommie, Y. R. Shen, and F. Wang, Nature **459**, 820 (2009).
[41] K. Mak, C. Lui, J. Shan, and T. Heinz, Phys. Rev. Lett. **102**, 256405 (2009).
[42] K. Zou, and J. Zhu, Phys. Rev. B **82**, 081407 (2010).
[43] K. Zou, F. Zhang, C. Clapp, A. H. MacDonald, and J. Zhu, Nano Letters **13**, 369 (2013).
[44] M. M. Lucchese, F. Stavale, E. H. M. Ferreira, C. Vilani, M. V. O. Moutinho, R. B. Capaz, C. A. Achete, and A. Jorio, Carbon **48**, 1592 (2010).

[45] A. Weisse, G. Wellein, A. Alvermann, and H. Fehske, Rev. Mod. Phys **78**, 275 (2006).
[46] S. Yuan, H. De Raedt, and M. I. Katsnelson, Phys. Rev. B **82**, 235409 (2010).
[47] E. V. Castro, K. S. Novoselov, S. V. Morozov, N. M. R. Peres, J. M. B. Lopes dos Santos, J. Nilsson, F. Guinea, A. K. Geim, and A. H. Castro Neto, J. Phys.: Condens. Matter **22** 175503 (2010).
[48] A weak n-dependence of screening $\kappa(n)$ arising from charge imbalance between the layers has been neglected.
[49] B. A. Lippmann and J. Schwinger, Phys. Rev. **79**, 469 (1950).
[50] Outside the intermediate density regime, the expression for the dc-conductivity must be generalized to account for band degeneracies; refer to SM for full details.

document